International Journal of Rock Mechanics & Mining Sciences 46 (2009) 272–280

Contents lists available at ScienceDirect

International Journal of Rock Mechanics & Mining Sciences

journal homepage: www.elsevier.com/locate/ijrmms

Point load tests and strength measurements for brittle spheres

Adrian R. Russell [a,*], David Muir Wood [b]

[a] School of Civil and Environmental Engineering, University of New South Wales, Sydney, NSW 2052, Australia
[b] Department of Civil Engineering, University of Bristol, Queen's Building, University Walk, Bristol BS8 1TR, UK

ARTICLE INFO

Article history:
Received 17 January 2008
Received in revised form
11 March 2008
Accepted 11 April 2008
Available online 5 June 2008

Keywords:
Point tests
Rocks
Brittle materials
Multiaxial failure
Microstructure
Compressive strength
Tensile strength

ABSTRACT

A multiaxial failure criterion for brittle materials is applied to a stress field analysis of a perfectly elastic sphere subjected to diametrically opposite normal forces that are uniformly distributed across small areas on the sphere's surface. Expressions are obtained for an intrinsic strength parameter of the material, as well as its unconfined compressive strength. An expression for the unconfined tensile strength is obtained by introducing an additional parameter accounting for the microstructural features of the material. The expressions indicate that failure initiates in the sphere where the ratio between the second deviatoric stress invariant and the first stress invariant is a maximum. Such a criterion does not coincide with the location of maximum tensile stress. The expressions are used to reinterpret published point load test results and predict unconfined compressive strengths. The configuration of the point load test as well as surface roughness and elastic properties of the pointer and samples are taken into account to establish the size of the area on which the point loads act. The predictions are in good agreement with measured values obtained directly using unconfined compressive strength tests. It is concluded that the point load test provides a more reliable estimate of the compressive strength than the tensile strength.

1. Introduction

The point load test has long been considered a useful tool to estimate strengths of brittle materials including rock [1–3]. The test is appealing, since little or no sample preparation is needed and the testing equipment is portable, allowing laboratory as well as field use. Samples can be of various shapes including cut cylindrical cores tested axially or diametrically, cut blocks, or irregular lumps (Fig. 1a). The stress fields within the differently shaped samples subjected to point loads are highly non-uniform. However, the stress fields along the axes of loading are broadly similar for the different shapes [1]. The unconfined compressive strength σ^c is obtained using the equation [3]

$$\sigma^c = CI_{s50}, \tag{1}$$

where I_{s50} is the corrected point load strength for a sample and is equal to f/d^2 multiplied by shape and size correction factors, f is the force causing failure, d is the equivalent sample diameter, and C is a constant which normally takes a value somewhere between 8.6 and 29, depending on rock type and the magnitude of I_{s50}. A more obvious tool for the measurement of σ^c is the unconfined compressive strength test which involves squashing a cylindrical sample between rigid and flat (and ideally frictionless) end platens rather than point loads (Fig. 1b). A uniform stress field develops within the sample and σ^c is found by dividing the failure load by the cross-sectional area of the sample. However, as the samples and loading equipment used in point loads tests are much more readily available than those used in unconfined compressive strength tests, the use of Eq. (1) and point load tests to determine σ^c continues to be widespread.

There has been much research on the point load test, albeit mostly empirical, to establish suitable values of C for the wide variety of rock types. Fener et al. [4] give a good summary of historical and recent work. However, due to the lack of an obvious connection between the test configuration, the stress fields which develop, and the mechanisms causing failure, theoretical explanations for the parameter C are rare.

One of the few attempts was made by Chau and Wong [5]. Their investigation was based on the major assumption that there exists a uniform tensile stress across the sample diameter connecting the point loads at the onset of failure. It was also assumed that the sample fails by the growth of microcracks along that diameter and subsequent tensile splitting. The tensile strength was determined (at least approximately) using Wijk's [6] equation

$$\sigma^t = B\frac{|f|}{d^2}, \tag{2}$$

* Corresponding author. Tel.: +61 2 9385 5035; fax: +61 2 9385 6139.
E-mail address: a.russell@unsw.edu.au (A.R. Russell).

1365-1609/$ - see front matter © 2008 Elsevier Ltd. All rights reserved.
doi:10.1016/j.ijrmms.2008.04.004

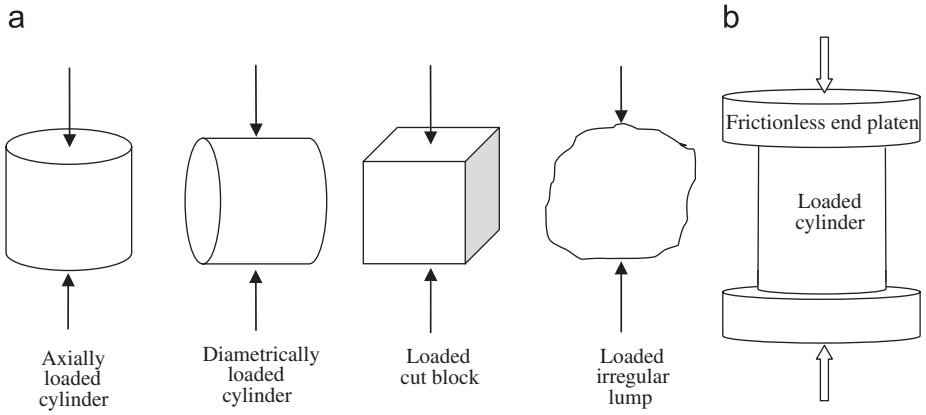

Fig. 1. Configurations of point load tests (a) and unconfined compressive strength test (b).

where B is a parameter that usually lies in the range 0.4–1.5 and depends on sample size, geometry and elastic properties. Chau and Wong [5] further assumed that the ratio between σ^c and σ^t is a material constant, having applied Costin's [7] three-dimensional (3D) microcrack growth criterion to compressive and tensile loading, along with consideration of experimental evidence reported in Goodman [8]. This enabled σ^c to be directly determined by multiplying σ^t by the constant. It is important to note that the work of Wijk [6] and Chau and Wei [9] shows that the tensile stress across the diameter is far from uniform. In fact, Chau and Wong [5] recognised the limited validity of this major assumption. Furthermore, Chau and Wong [5] did not consider the size of the quasi-point load contacts with the sample, which significantly influences the stress field, especially along the sample diameter.

In the present investigation, a new analytical approach to the generation of the internal stress field is presented. The multiaxial failure criterion for brittle materials proposed by Christensen [10], which includes two material constants to characterise the strength of the material, is applied to the stress field within an elastic sphere submitted to a point load test. Consideration is given to the contact areas on which the point loads act and how this influences failure in the diametrically loaded sphere. Theoretical expressions for σ^c and σ^t are developed and compared with results of point load tests for a variety of rock types. The sphere provides a simple 3D geometry which forms a reference against which other (more or less irregular) sample shapes can be compared (Fig. 1a).

2. Linking stress fields to failure

The solutions of Hiramatsu and Oka [1] allow the complete stress field in a diametrically loaded sphere to be obtained, as shown in Fig. 2. (The numerical code used in this investigation has been validated by reproducing the stress fields in Ref. [11].) In these solutions, the forces are assumed to act normal to the surface of the sphere on small areas defined by the subtended angle θ_0 (Fig. 3). The results shown in Fig. 2 are for the case in which Poisson's ratio $\mu = 0.25$ and Young's modulus $E = 90\,\text{GPa}$, assuming circular contact areas at each end of the loaded diameter bounded by $\theta_0 = \pi/36$. The stress field is represented by four contour plots of the normalised quantities $\pi R^2\sigma_r/f$, $\pi R^2\sigma_\theta/f$, $\pi R^2\sigma_\psi/f$ and $\pi R^2\tau_{r\theta}/f$ on sections through the sphere, where $R = d/2$ is the radius of the sphere, σ_r, σ_θ, σ_ψ and $\tau_{r\theta}$ are normal and shear stress components defined using spherical polar coordinates (Fig. 4) and force f is negative for pushing (compression). The other components of shear stress, on meridional planes, are zero, by symmetry. Tensile stresses are taken as positive: the distribution of $\pi R^2\sigma_\theta/f$ along the diameter of the sphere through which the centre of the 'point' loads act indicates that a localised negative peak normalised value, which corresponds to the peak tensile principal stress, exists at $r/R = 0.84$. For a wider range of elastic constants and values of θ_0 the peak is located somewhere around $r/R = 0.7$–0.9 [9].

The mechanisms causing failure can be investigated further and the appropriateness of Eqs. (1) and (2) assessed by assuming an appropriate failure criterion. As point load tests considered here are performed on pieces of rock (and even on individual sand or gravel particles), the criterion must be suited to brittle geomaterials. However, the multiaxial material failure characterisation of many engineering materials, not just brittle geomaterials, is not well advanced [10]. Exceptions include concrete (for example, Ref. [12]) and ductile metals. In this study, the simple two-parameter multiaxial failure criterion for brittle materials proposed in Ref. [10] are assumed to apply.

The criterion states that a material is not at failure when

$$\frac{\chi\kappa}{\sqrt{3}}I_1 + (1+\chi)^2 J_2 < \frac{\kappa^2}{1+\chi}, \tag{3}$$

where $J_2 = I_1^2/3 - I_2$ is the second invariant of the deviatoric stress tensor, I_1 and I_2 are the first and second invariants of the stress tensor, and tensile stresses being taken as positive. Writing the stress tensor in the form

$$\begin{bmatrix} \sigma_x & \tau_{xy} & \tau_{xz} \\ \tau_{xy} & \sigma_y & \tau_{yz} \\ \tau_{xz} & \tau_{yz} & \sigma_z \end{bmatrix}, \tag{4}$$

the invariants I_1 and I_2 are defined as

$$I_1 = \sigma_x + \sigma_y + \sigma_z$$

and

$$I_2 = \sigma_x\sigma_y + \sigma_x\sigma_z + \sigma_y\sigma_z - \tau_{xy}^2 - \tau_{xz}^2 - \tau_{yz}^2. \tag{5}$$

For unconfined compression, where σ^c is the applied uniaxial stress at failure, $I_1 = \sigma^c$, $I_2 = 0$ and $J_2 = (\sigma^c)^2/3$.

The criterion in Eq. (3) is a modified form of the von Mises criterion, the modification surrounding the inclusion of I_1 in the first part of the expressions. The parameter χ is a dimensionless shape parameter and represents the ratio between the characteristic uniaxial compressive and tensile strengths, σ^c and σ^t respectively, through

$$\chi = \frac{|\sigma^c|}{\sigma^t} - 1. \tag{6}$$

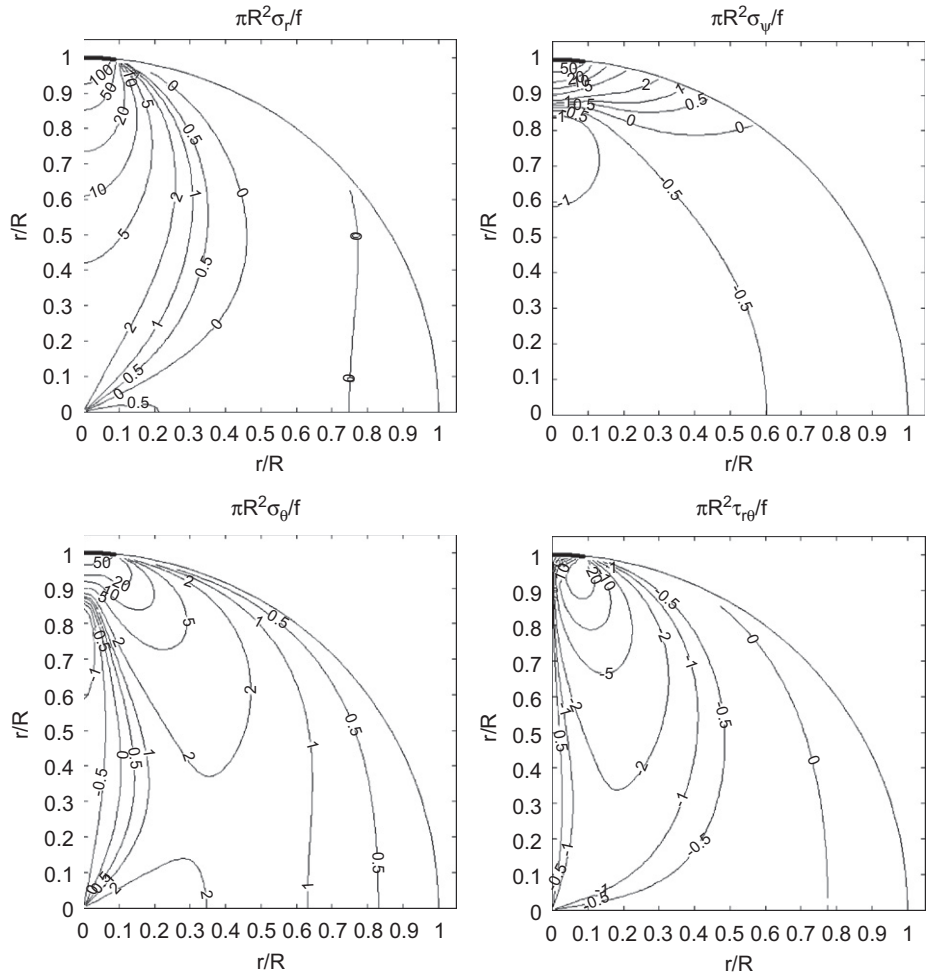

Fig. 2. Normalised stress fields $\pi R^2\sigma_r/f$, $\pi R^2\sigma_\theta/f$, $\pi R^2\sigma_\psi/f$ and $\pi R^2\tau_{r\theta}/f$ for diametrically opposite contact forces f applied to an area bounded by $\theta_0 = \pi/36$ and for the elastic properties $\mu = 0.25$ and $E = 90$ GPa. The bold line near the top of the sphere indicates the extent of the surface over which the contact force is uniformly applied.

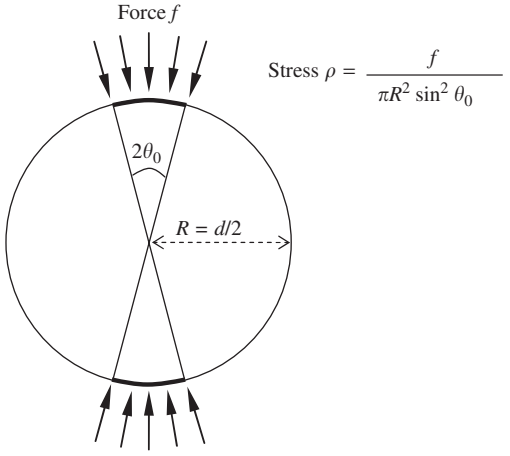

Fig. 3. Force f acts normal to sphere surface on an area defined by the angle θ_0. The equivalent stress acting on the area is ρ. The stress components in the sphere are defined using the spherical polar coordinates $r{\sim}\theta{\sim}\psi$ in Fig. 4.

The parameter κ is a positive scale parameter defined as

$$\kappa = \frac{1+\chi}{\sqrt{3}}|\sigma^c|. \tag{7}$$

The characteristic strengths are then

$$\sigma^c = -\frac{\sqrt{3}\kappa}{1+\chi} \text{ and } \sigma^t = \frac{\sqrt{3}\kappa}{(1+\chi)^2}. \tag{8}$$

In explaining the physical meanings of χ and κ, Christensen [10] points out that when $\chi = 0$ the material behaviour at failure is of the von Mises type, as the criterion in Eq. (3) simplifies to $J_2 < \kappa^2$ and the parameter κ solely controls the yield strength. When $\chi = 0$ the criterion defines a failure surface in 3D stress space that has the shape of a right circular cylinder, symmetrical about the hydrostatic axis, and with radius $\sqrt{2}\kappa$. When $\chi > 0$, Eq. (3) defines a failure surface in the 3D stress space that has the shape of a revolved paraboloid symmetric about the hydrostatic axis. When $\chi \to \infty$, however, the material is unable to sustain any load, as disintegration occurs. Based on these characteristics, Christensen [10] referred to κ as an "intrinsic strength" and χ as a "microstructure parameter". Christensen [10] surmised that κ is a measure of the strength of the material having no microstructural damage and must be related to atomic scale properties. Christensen [10] also proposed that χ represents the effects of microstructural deviations from the ideal. Eq. (3) remains an empirical expression with two degrees of freedom: the attribution of microstructural origins to κ and χ is not actually supported by any atomic scale studies.

Fig. 5 shows normalised sections though the failure surface along the hydrostatic axis for different values of χ. The normalised

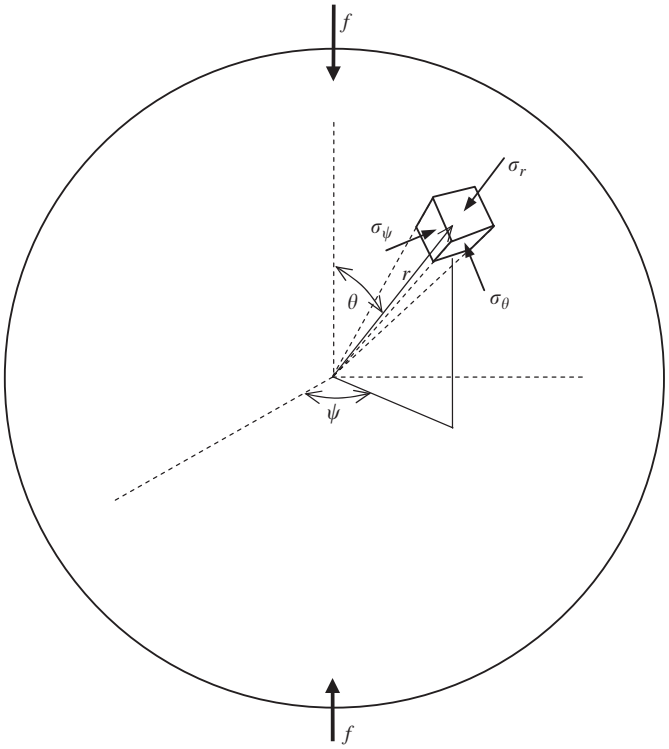

Fig. 4. Spherical polar coordinates $r{\sim}\theta{\sim}\psi$ and orthogonal normal stresses σ_r, σ_θ and σ_ψ. r is the distance from the sphere centre to the location of interest and θ is the angle r subtends from the line through which the two forces f act. The corresponding shear stresses $\tau_{r\theta}$, $\tau_{\theta\psi}$ and $\tau_{r\psi}$ have not been shown for clarity. Only $\tau_{r\theta}$ has a finite value. $\tau_{\theta\psi}$ and $\tau_{r\psi}$ are zero due to symmetry.

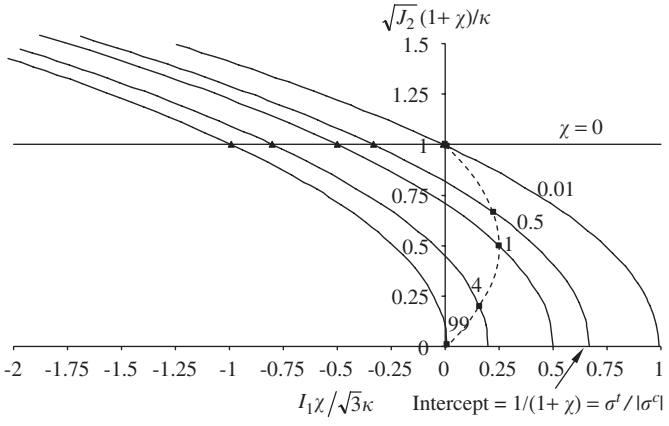

Fig. 5. Normalised sections though the failure surface defined by the criterion in Eq. (3) for different values of χ. The triangular and square symbols represent failure points for unconfined compression and extension, respectively.

quantities $I_1\chi/\sqrt{3}\kappa$ and $\sqrt{J_2}(1+\chi)/\kappa$ have been selected for the horizontal (x) and vertical (y) axes, respectively, so that the sections depend only on χ and not on κ. When $\chi>0$ the sections intercept the hydrostatic axis at $1/(1+\chi)$, representing the ratio $\sigma^t/|\sigma^c|$. For all values of χ sections of the surfaces through the deviatoric plane perpendicular to the hydrostatic axis are circular. Triangular symbols on the normalised sections in Fig. 5 represent failure points for unconfined compression, which happen to lie on the horizontal line $y=1$ with x ordinates given by $x=-\chi/(1+\chi)$, such that x lies within the limits $-1\leqslant x\leqslant 0$ for all values of χ. Square symbols represent failure points for unconfined tension, which happen to lie on a parabola defined by $x=y-y^2$, as indicated by the dashed line, where x and y coordinates are given by $x=\chi/(1+\chi)^2$ and $y=1/(1+\chi)$, such that y lies within the limits $0\leqslant y\leqslant 1$ for all values of χ.

3. An analytical study

The mineral of which the sphere is composed has a certain available strength that is characterised by the value of κ. When subjected to contact forces the multiaxial stress state within the sphere will use up or *mobilise* a certain amount of this *available* strength, the amount denoted by κ_{mob}. Forcing equality in the failure criterion and replacing κ with κ_{mob} gives the quadratic expression

$$\kappa_{\mathrm{mob}}^2-\frac{(1+\chi)\chi I_1}{\sqrt{3}}\kappa_{\mathrm{mob}}-(1+\chi)^3J_2=0. \tag{9}$$

There are two possible solutions to the quadratic Eq. (9) for κ_{mob}. The one that is relevant is the one that gives a positive value for κ_{mob}

$$\kappa_{\mathrm{mob}}=\frac{(1+\chi)\chi I_1}{2\sqrt{3}}\left(1-\sqrt{1+12\left(\frac{1}{\chi^2}+\frac{1}{\chi}\right)\frac{J_2}{I_1^2}}\right). \tag{10}$$

Goodman [8] presented tensile and compressive strengths for a range of rock types indicating that, if the above failure criterion and Eq. (8) apply, $1+\chi$ varies from about 10 to 170. For values of $\chi\gg 1$ the second part under the square root in Eq. (10) is much smaller than unity so that the approximation $\sqrt{1+\Delta}=1+\Delta/2$ can be used to give a simpler approximate expression for κ_{mob}

$$\kappa_{\mathrm{mob}}\approx-\frac{\sqrt{3}(1+\chi)^2}{\chi}\frac{J_2}{I_1}. \tag{11}$$

Since the sphere is assumed to be elastic, κ_{mob} at any point will be proportional to the applied load. As the applied load is increased, failure of the sphere will occur when the *maximum* κ_{mob} attains a value equal to the available strength κ. The location of maximum κ_{mob} is where failure will initiate which, from Eq. (11), is also the location where the ratio $-J_2/I_1$ is a maximum (as long as $\chi\gg 1$). By replacing κ_{mob} in Eq. (11) with κ and $-J_2/I_1$ with its maximum value denoted as $(-J_2/I_1)_{\max}$, and by combining Eqs. (11) and (8), alternate expressions for the intrinsic and characteristic strengths at failure are obtained

$$\kappa=\frac{\sqrt{3}(1+\chi)^2}{\chi}\left(-\frac{J_2}{I_1}\right)_{\max},$$
$$\sigma^{\mathrm{c}}=-\frac{3(1+\chi)}{\chi}\left(-\frac{J_2}{I_1}\right)_{\max},\quad \sigma^{\mathrm{t}}=\frac{3}{\chi}\left(-\frac{J_2}{I_1}\right)_{\max}. \tag{12}$$

Note that the $=$ sign has been used in the three parts of Eq. (12), and in the remaining equations throughout this paper, even though small approximations may be contained in their derivation. For large values of χ, σ^{c} may be simplified further to give

$$\sigma^{\mathrm{c}}=-3\left(-\frac{J_2}{I_1}\right)_{\max}. \tag{13}$$

Eq. (13) highlights the fact that for rocks, or more generally any material having a large value of χ, σ^{c} is virtually independent of χ and κ, but is totally dependant on the stress field in the sample at the onset of failure.

Symmetrical maxima of κ_{mob} (or $-J_2/I_1$) are located on the diameter connecting the centres of the loading areas and in the vicinity of the force contacts. Also, in the vicinity of the force contacts, when θ_0 is small and where ρ represents the average pressure provided by the contact force f divided by the small area on which it acts (Fig. 3), i.e.,

$$\rho=\frac{f}{\pi R^2\sin^2\theta_0}, \tag{14}$$

the stresses given by the solutions of Hiramatsu and Oka [1] are virtually identical to those for a uniform pressure ρ acting on a circular area of radius ω on an elastic half-space. Solutions for the

stresses within the half-space along the line normal to and through the centre of the loaded area are therefore of interest as they are much simpler than those of Hiramatsu and Oka [1] and lend themselves to simple mathematical manipulation. The solutions are [13, Chapter 7]

$$\sigma_r = \left[1 - \frac{1}{(1+(z/\omega)^2)^{3/2}}\right]\rho,$$
$$\sigma_\theta = \sigma_\psi = \left[\frac{1}{2} + \mu - \frac{1+\mu}{(1+(z/\omega)^2)^{1/2}} + \frac{1}{2(1+(z/\omega)^2)^{3/2}}\right]\rho, \quad (15)$$

where z is the distance below the centre of the area. The notations for the principal stresses σ_r, σ_θ and σ_ψ have been used to maintain similarity with those used for the stresses immediately below the concentrated diametrically opposite forces f acting on a sphere (Fig. 4); σ_r is the principal stress along the loaded diameter of the sphere, and σ_θ and σ_ψ are the two orthogonal principal stresses. The expressions in Eq. (15) can be substituted into I_1 and J_2 and then into Eq. (11) to arrive at an approximate expression for κ_{mob}, which can be differentiated with respect to z/ω to show that κ_{mob} is a maximum when

$$\frac{z}{\omega} = \frac{\sqrt{(8\mu^2+40\mu+50)\left(20\mu+109-3\sqrt{309+120\mu-8\mu^2}\right)}}{8\mu^2+40\mu+50}. \quad (16)$$

The ratio z/ω in Eq. (16) takes a value that varies between about 1.03 and 0.94 for values of μ that vary between 0.1 and 0.4. Due to this weak dependence on μ, it can be reasonably assumed that κ_{mob} is always a maximum when $z/\omega = 1$.

Using this result, expressions for the stress invariants at the point where κ_{mob} is a maximum within a sphere, i.e., $R\tan\theta_0$ below the centre of the contact (corresponding to $z/\omega = 1$), can be obtained. We note that for small θ_0, $\tan\theta_0 \approx \sin\theta_0$, thus the depth below the loaded area of radius $R\sin\theta_0$ to the point of maximum κ_{mob} is approximately equal to the radius of the loaded area, and therefore

$$I_1 = \left(2-\sqrt{2}\right)(1+\mu)\rho,$$
$$J_2 = \left(\frac{3}{32} + \frac{\sqrt{2}}{24} + \left(\frac{\sqrt{2}}{12} - \frac{1}{4}\right)\mu + \left(\frac{1}{2} - \frac{\sqrt{2}}{3}\right)\mu^2\right)\rho^2. \quad (17)$$

Eq. (17) can be substituted into Eqs. (12) and (13) to obtain complete (and only slightly approximate) expressions for the intrinsic and characteristic strengths

$$\kappa = -\frac{\sqrt{3}(1+\chi)^2}{\chi} \times \frac{\left(\frac{3}{32} + \frac{\sqrt{2}}{24} + \left(\frac{\sqrt{2}}{12} - \frac{1}{4}\right)\mu + \left(\frac{1}{2} - \frac{\sqrt{2}}{3}\right)\mu^2\right)}{\left(2-\sqrt{2}\right)(1+\mu)} \times \frac{f}{\pi R^2 \sin^2\theta_0}, \quad (18)$$

$$\sigma^c = 3\frac{\left(\frac{3}{32} + \frac{\sqrt{2}}{24} + \left(\frac{\sqrt{2}}{12} - \frac{1}{4}\right)\mu + \left(\frac{1}{2} - \frac{\sqrt{2}}{3}\right)\mu^2\right)}{\left(2-\sqrt{2}\right)(1+\mu)} \times \frac{f}{\pi R^2 \sin^2\theta_0}, \quad (19)$$

$$\sigma^t = -\frac{3}{\chi}\frac{\left(\frac{3}{32} + \frac{\sqrt{2}}{24} + \left(\frac{\sqrt{2}}{12} - \frac{1}{4}\right)\mu + \left(\frac{1}{2} - \frac{\sqrt{2}}{3}\right)\mu^2\right)}{\left(2-\sqrt{2}\right)(1+\mu)} \times \frac{f}{\pi R^2 \sin^2\theta_0}. \quad (20)$$

In applying Eqs. (18)–(20) it is necessary to know the size of the contact areas on which the forces f are applied, defined by θ_0, which can be determined using Hertzian contact theory. Surface roughness can also be considered, for example using the solutions of Bahrami et al. [14], as will be demonstrated following a parametric study.

4. A parametric study

A parametric study will now be conducted and a back-calculation of material strength will be performed using the point load strength test result for an individual quartz sand particle presented in Ref. [15]. Using data from Fig. 2 of Nakata et al. [15], the contact force at failure for a particle of an average diameter of $d = 1.4$ mm was observed to be $f = -165$ N, with the negative indicating the force is compressive. This information, along with assumed elastic properties for quartz $\mu = 0.08$ and $E = 90$ GPa [16] and an assumed contact area bound by $\theta_0 = \pi/36$, may be substituted into the solutions of Hiramatsu and Oka [1] to give the stress fields within the particle at the onset of failure. Although the stress fields are not presented here, a local negative peak in the normalised tensile stress of $\pi R^2\sigma_\theta/f = -3.4$ was found to exist at $r/R = 0.84$, corresponding to a peak tensile stress of $\sigma_\theta = 364$ MPa. A very large normalised compressive stress of $\pi R^2\sigma_r/f = 132$, corresponding to $\sigma_r = -14{,}100$ MPa (which is equal to ρ), exists adjacent to the point load contact, as expected.

Using this stress field, a contour plot of κ_{mob} may be drawn for different values of χ. The χ values considered here are: 19, 49, 99, 199; which have an order of magnitude typical for geological materials [8,10]. The contour plot of κ_{mob} for $\chi = 99$ is presented in Fig. 6. For $\chi = 99$ a maximum κ_{mob}, which represents the intrinsic strength, was found to be $\kappa = 520$ GPa and located at $r/R = 0.91$ directly below the centre of the area on which the contact force is applied. For $\chi = 19$, 49 and 199 the maxima were found to be

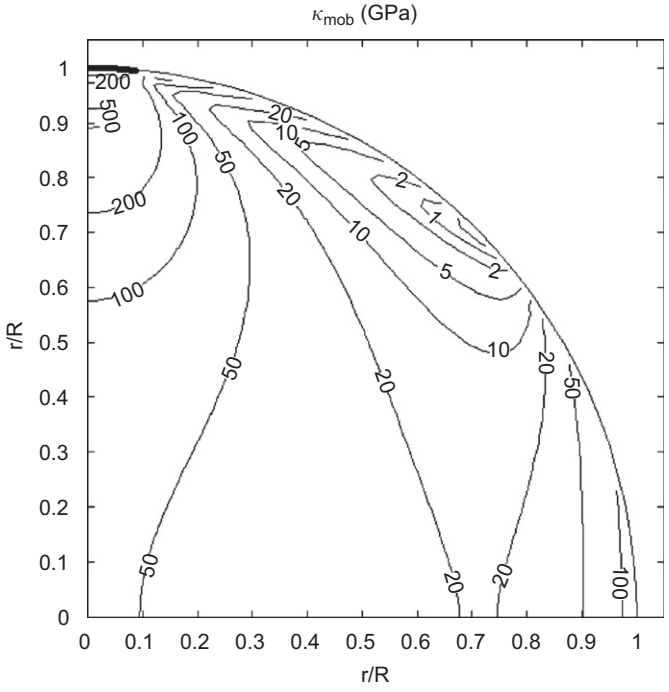

Fig. 6. A contour plot of κ_{mob} for $\chi = 99$, diametrically opposite contact forces of $f = -165$ N, applied to an area bounded by $\theta_0 = \pi/36$, $d = 1.4$ mm, $\mu = 0.08$ and $E = 90$ GPa. The bold line near the top of the sphere indicates the extent of the surface over which the contact force is uniformly applied.

$\kappa = 110$, 260, 1050 GPa, respectively, each occurring at almost identical locations within the particle—directly below the centre of the contact area where $r/R = 0.91$. Notice that maximum κ_{mob} occurs at locations which are slightly different from the locations of the maximum tensile stress. Also notice that the maximum κ_{mob} is located at a distance of $R\tan\theta_0$ below the centre of the contact, as expected. Table 1 lists the κ_{mob} maxima as κ and also lists 'exact' values of σ^c and σ^t determined using Eq. (8). The data confirm that κ is 230–23,000 times larger than σ^t, a large range dependant on χ although of the correct order of magnitude expected for geological materials [10]. For example, the theoretical tensile strength of a homogenous and flawless piece of aggregate has been estimated to be 1000 times larger than the actual measured tensile strength [17].

Also presented in Table 1 for comparison are the 'approximate' values for κ, σ^c and σ^t, obtained using Eqs. (18)–(20). To explore the sensitivity of Eqs. (18)–(20) for a range of values for μ and θ_0, Tables 2–4 present other sets of results but for $\mu = 0.25$ and $\theta_0 = \pi/36$, $\mu = 0.08$ and $\theta_0 = \pi/180$, and $\mu = 0.25$ and $\theta_0 = \pi/180$, respectively.

Clearly, the approximate values of the intrinsic and characteristic strengths κ, σ^c and σ^t are within a few percent of the exact values. It may be concluded that Eqs. (18)–(20) are accurate approximations.

From the data presented in Tables 1–4 it is clear that σ^t is heavily influenced by χ. In other words, adopting the ideas of Christensen [10], it is heavily influenced by the microstructure of the particle. However, Eq. (2) (assuming $B = 1$) would give a single value of $\sigma^t = 84$ MPa for the point load test of Nakata et al. [15] used as an example here, giving no consideration to the microstructure. It may be concluded that Eq. (2) is unsuitable to determine (even approximately) a characteristic tensile strength. In contrast, the data presented in Tables 1–4 indicate that σ^c is largely unaffected by the microstructure (the value of χ), but is highly dependant on μ and θ_0. This suggests that the point load test is better suited to determine a characteristic compressive

Table 1
Exact and approximate strength characteristics for $f = -165$ N, $d = 1.4$ mm, $\mu = 0.08$ and $\theta_0 = \pi/36$

χ	κ (GPa)		σ^c (MPa)		σ^t (MPa)	
	Exact (L) & approximate from Eq. (18) (R)		Exact (L) & approximate from Eq. (19) (R)		Exact (L) & approximate from Eq. (20) (R)	
19	110	116	−9090	−9520	460.0	501.0
49	260	280	−9080	−9520	180.0	194.0
99	520	555	−9060	−9520	91.1	96.2
199	1050	1100	−9060	−9520	45.3	47.8

Table 2
Exact and approximate strength characteristics for $f = -165$ N, $d = 1.4$ mm, $\mu = 0.25$ and $\theta_0 = \pi/36$

χ	κ (GPa)		σ^c (MPa)		σ^t (MPa)	
	Exact (L) & approximate from Eq. (18) (R)		Exact (L) & approximate from Eq. (19) (R)		Exact (L) & approximate from Eq. (20) (R)	
19	81.2	85.3	−7030	−7020	351.0	369.0
49	201.0	207.0	−6960	−7020	139.0	143.0
99	401.0	409.0	−6940	−7020	69.4	70.9
199	800.0	815.0	−6920	−7020	34.8	35.3

Table 3
Exact and approximate strength characteristics for $f = -165$ N, $d = 1.4$ mm, $\mu = 0.08$ and $\theta_0 = \pi/180$

χ	κ (GPa)		σ^c (MPa)		σ^t (MPa)	
	Exact (L) & approximate from Eq. (18) (R)		Exact (L) & approximate from Eq. (19) (R)		Exact (L) & approximate from Eq. (20) (R)	
19	2690	2890	−233,000	−237,000	11,700	12,500
49	6710	6990	−232,000	−237,000	4650	4850
99	13,400	13,800	−231,000	−237,000	2310	2400
199	26,700	27,600	−231,000	−237,000	1160	1190

Table 4
Exact and approximate strength characteristics for $f = -165$ N, $d = 1.4$ mm, $\mu = 0.25$ and $\theta_0 = \pi/180$

χ	κ (GPa)		σ^c (MPa)		σ^t (MPa)	
	Exact (L) & approximate from Eq. (18) (R)		Exact (L) & approximate from Eq. (19) (R)		Exact (L) & approximate from Eq. (20) (R)	
19	2010	2130	−174,000	−175,000	8700	9210
49	4940	5160	−171,000	−175,000	3430	3570
99	9850	10,200	−170,000	−175,000	1700	1770
199	19,600	20,300	−169,000	−175,000	847	880

strength than a tensile strength, as long as μ and θ_0 are known or can be estimated. An application of this theoretical result to point load tests performed on a wide variety of rock types to obtain characteristic compressive strengths will now be presented.

5. Application

We return to the point load test. Provided that C is known, σ^c can be determined using Eq. (1) after I_{s50} is measured in the test. An assumption may then be made for χ to get κ and σ^t from Eqs. (6) and (7). It is noted that σ^c and σ^t may be measured directly using unconfined compression and extension tests, so that χ and κ may be determined using Eqs. (6) and (7) without making any assumptions. However, the focus of this study is on the theoretical interpretation of the point load test when results of unconfined compression and extension tests are unavailable.

An expression for C is found by rearranging Eqs. (1) and (19)

$$C = 3\frac{\left(\frac{3}{32}+\frac{\sqrt{2}}{24}+\left(\frac{\sqrt{2}}{12}-\frac{1}{4}\right)\mu+\left(\frac{1}{2}-\frac{\sqrt{2}}{3}\right)\mu^2\right)}{\left(2-\sqrt{2}\right)(1+\mu)}\frac{4}{\pi\sin^2\theta_0}. \quad (21)$$

Clearly, μ and θ_0 have a major influence on C, and therefore contribute to the uncertainty in C that is so often observed. For example, assuming $\theta_0 = \pi/36$, C varies from 119 to 11.3 as μ varies from 0.05 to 0.45. Similarly, assuming $\mu = 0.25$, C varies from 66 to 7.5 as θ_0 varies from $\pi/36$ to $\pi/12$. It is clear from Eqs. (1), (7) and (6) that σ^c, κ and σ^t are proportional to C (for a given χ) and therefore are also highly dependant on μ and θ_0, as can also be observed in Tables 1–4.

A reasonable estimate of μ may be assumed or obtained from published tables if it cannot be measured experimentally. However, to establish a suitable value for θ_0, it is necessary to consider the geometry of a point load test (Fig. 7a). Typically the pointer is made of tungsten carbide or hardened steel with a smooth and spherically curved tip of $r_1 = 5$ mm radius [3]. As the stress fields within the vicinity of the contact points where failure initiates are largely independent of sample shape [1], it is assumed the stress field analysis conducted above for spherical samples is applicable to the other shapes used for point load tests. Samples can in principle also be of any size although only I_{s50} values will be considered here in order to remove the effects of size in the present analysis. The radius of the spherical rock samples is therefore taken to be $r_2 = 25$ mm (Fig. 7a). θ_0 also depends on the surface roughness of the rock samples in the area of contact with the pointers, which in turn depends on many factors including rock type, mineralogy and composition as well as the method of cutting and removing the sample from the ground.

The theoretical work of Bahrami et al. [14], which studies the mechanics of a rough elastic sphere in contact with a smooth elastic sphere, is summarised here. This work allows an expression for θ_0 to be obtained as a function of surface roughness, using an extension of Hertzian contact theory for smooth elastic spheres. For smooth spheres the radius of the contact area is

$$r_H = \left(\frac{3|f|r'}{4E'}\right)^{1/3}, \quad (22)$$

where r' and E' are the effective radius of curvature and effective elastic modulus, respectively, defined by

$$\frac{1}{r'} = \frac{1}{r_1}+\frac{1}{r_2} \text{ and } \frac{1}{E'} = \frac{1-\mu_1^2}{E_1}+\frac{1-\mu_2^2}{E_2}, \quad (23)$$

in which r_1 and r_2 are the radii of the two spheres in contact, and E_1, E_2, μ_1 and μ_2 are the elastic properties of the two spheres in contact (see Fig. 7a).

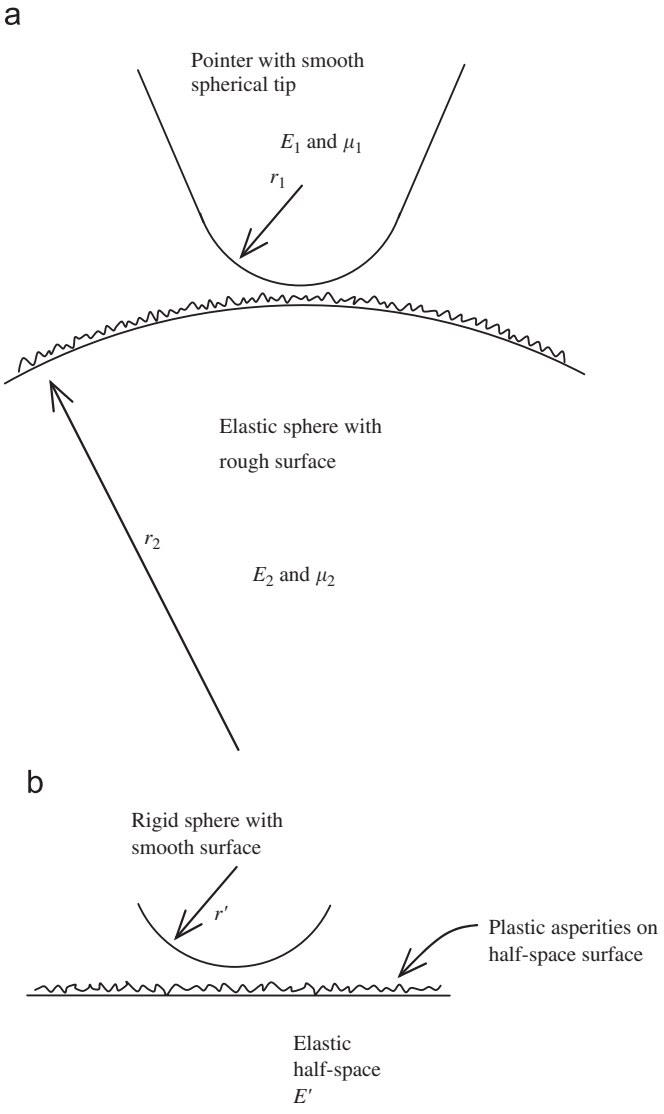

Fig. 7. The geometry of a point load test (a) and an equivalent system (b).

To take into account surface roughness, Bahrami et al. [14] assumed that roughness is isotropic and follows a Gaussian distribution. They also assumed that the deformation mode of the asperities is plastic, even though the deformation of the substrate within the spheres is elastic. The geometry of a contact was converted to an equivalent system as shown in Fig. 7b, where a rigid and smooth single sphere of radius r' pushes against an elastic half-space of modulus E', and the asperities are treated as a plastic layer on the surface of the elastic half-space.

Two nondimensional parameters were introduced

$$\alpha = \frac{sr'}{r_H^2} \text{ and } \beta = \frac{E'}{H_{mic}}\sqrt{\frac{r'}{s}}, \quad (24)$$

where s is the root mean square of the asperity heights making up the surface roughness and has dimensions of length. H_{mic} is the effective microhardness of the asperities and has units of stress. Complicated computations were then undertaken by Bahrami et al. [14] who found that the pressure distribution across the contact area is not uniform. It has a maximum value of P_0 at the centre and reduces away from the centre as a function of α and β.

Table 5
Data from Kahraman [14] including averages of measured σ^c values for a range of rock types, together with predicted σ^c values obtained using Eqs. (1) and (21)

Rock type	σ^c (MPa) (average of measured values)	I_{s50} (MPa)	Density (Mg/m^3)	p-wave velocity (km/s)	μ (assumed)	E (GPa)	σ^c (MPa) (predicted using Eqs. (1) and (21))
Dolomite	68.0	4.32	2.92	6.3	0.30	86.1	48.5
Sandstone-1	149.2	13.83	3.00	4.6	0.30	47.2	140.6
Sandstone-2	45.2	4.57	2.77	4.5	0.30	41.7	49.4
Altered sandstone	20.1	1.32	2.55	2.0	0.15	9.7	18.4
Limestone	51.3	5.61	2.74	5.4	0.25	66.6	66.8
Marl	39.5	3.35	2.20	3.1	0.25	17.6	38.4
Diabase	110.9	12.66	2.96	5.2	0.40	37.4	107.4
Serpentine	69.1	7.14	2.88	2.9	0.45	6.4	48.9
Limestone	123.8	6.65	2.73	5.3	0.25	63.9	78.5
Clayed limestone	45.1	5.73	2.42	3.3	0.45	6.9	40.9
Hematite	61.8	8.26	3.61	2.8	0.45	7.5	56.6
Metasandstone	25.7	5.25	2.73	5.2	0.45	19.5	41.8
Serpentine	54.3	16.21	2.63	5.0	0.45	17.3	113.6
Limestone	15.7	1.40	1.86	2.2	0.25	7.5	16.1
Limestone	85.2	9.80	2.71	5.5	0.25	68.3	113.8
Sandstone	70.5	7.75	2.56	3.7	0.30	26.0	78.9
Limestone	42.1	5.44	2.71	4.7	0.25	49.9	64.1
Dolomite	96.3	12.01	2.98	5.6	0.30	69.4	126.4
Limestone	49.9	3.31	2.66	4.1	0.25	37.3	39.4
Limestone	76.1	8.82	2.96	5.6	0.25	77.4	103.5
Gravelled limestone	36.1	3.11	2.61	3.3	0.25	23.7	36.4
Limestone	68.4	7.00	2.81	5.0	0.25	58.5	82.1
Marl	64.9	3.60	2.45	3.4	0.25	23.6	41.8
Marl	13.5	2.13	2.03	1.5	0.25	3.8	22.3
Marl	21.4	1.73	1.91	1.9	0.25	5.7	19.2
Tuff	10.1	1.43	1.85	1.2	0.25	2.2	14.7
Marl	10.5	0.57	1.83	1.0	0.25	1.5	6.2

However, for simplicity in this investigation, the solutions of Bahrami et al. [14] have been applied in order to estimate the radius of the contact area even though, in our stress field analyses, a uniform distribution of pressure over the area of contact has been assumed, and this assumption of uniform contact pressure has been taken through to the approximate expressions for intrinsic and characteristic strengths in Eqs. (18)–(20).

The maximum nondimensional contact pressure P_0' as well as the nondimensional contact radius may be approximated (very closely) using the following expressions, as found in Ref. [14] after fitting curves to the computed results

$$P_0' = \frac{1}{1 + 1.22\alpha\beta^{-0.16}}, \tag{25}$$

$$r_L' = \begin{cases} 1.605\Big/\sqrt{P_0'} \text{ for } 0.01 \leqslant P_0' \leqslant 0.47, \\ 3.51 - 2.51P_0' \text{ for } 0.47 \leqslant P_0' \leqslant 1. \end{cases} \tag{26}$$

The actual contact radius r_L and therefore θ_0 are then given by the following expressions

$$r_L = r_L' r_H, \tag{27}$$

and

$$\tan\theta_0 = \frac{r_L}{R}, \tag{28}$$

where R is the radius of the sphere. The point load test data presented in Kahraman [18], summarised in Table 5, were used to observe the accuracy and predictive capability of this approach. The data include a list of mean I_{s50} values for a wide variety of rock types subjected to point load tests. Also given are mean values of σ^c for each rock type, determined directly by conducting unconfined compressive strength tests on cylindrical samples. Only the rock types in Kahraman [18] for which density (ρ_d) and p-wave velocity (V_p) were also given were used here, enabling the p-wave modulus (M) to be obtained through

$$M = \rho_d V_p^2. \tag{29}$$

With an assumed value of μ typical of each rock type, Young's modulus could then be determined through

$$E = \frac{(1+\mu)(1-2\mu)}{(1-\mu)}M. \tag{30}$$

Other assumptions were made in order to establish θ_0. The elastic properties of the pointer were assumed to be $E = 700$ GPa and $\mu = 0.25$, typical for tungsten carbide, and it was assumed that $H_{mic} = E'$. Finally, it was assumed that $s = 2.5$ mm (5% of the sample diameter). These latter two assumptions may be very far from reality; in particular, s would be much lower for a smoothly cut surface and higher for a broken or roughly cut surface. In any case, the predicted and the average measured σ^c values in Table 5, which are also plotted in Fig. 8, are in reasonable agreement, with a regression coefficient of $r = 0.84$. The bulk of the predicted values of σ^c lie within 50% of the averages of the measured values, shown by the dashed error lines.

This approach to theoretical interpretation of point load test results is considered to be superior to empirical approaches, because a single equation applies to all rock types. In contrast, in developing empirical expressions between I_{s50} and measured average σ^c values, it was necessary for Kahraman [18] to split the data into two categories: data for coal measure rocks and data for other rocks. Very different empirical expressions were found for each category, and the regression coefficients were 0.93 and 0.85, respectively, not much better than that found here based on a theoretical analysis. Of course, the regression coefficient found here could be increased and a better fit between theory and experiment obtained if more accurate knowledge of elastic

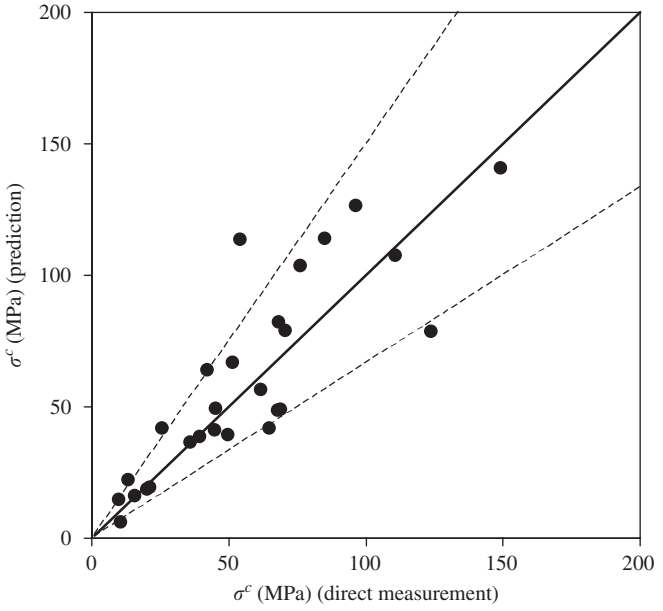

Fig. 8. Predicted versus measured values of σ^c: dashed lines indicate $\pm 50\%$ range.

properties and surface roughness were available and if the non-uniform contact pressure were taken into account.

6. Conclusion

Point load tests are regularly used to deduce the strengths of brittle geomaterials such as rocks and concrete. Analysis of the stress state in spherical elastic samples resulting from diametral loading applied over a small contact area around the nominal point of contact has allowed us to estimate the mobilisation of failure according to a recently established multiaxial failure criterion for brittle materials. This nonlinear failure criterion is described in terms of two parameters which can be linked to the uniaxial compressive and tensile strengths of the material. A point load test inevitably only produces a single result and it is thus only possible to deduce one strength if an assumption is made about either the other strength (for example, assuming a value for the ratio of compressive and tensile strengths) or about the shape of the multiaxial failure criterion. The interpretation of the stress distributions reported here suggests that the nature of this failure criterion implies that the point load test provides a much more reliable estimate of the compressive strength than the tensile strength—the value deduced is rather insensitive to many of the uncertainties of the elastic properties of the sample, the detail of the contact between the loading point and the sample, and the shape of the failure criterion. It is concluded that the use of such point load tests for the estimation of *tensile* strengths must be somewhat unreliable.

References

[1] Hiramatsu Y, Oka Y. Determination of the tensile strength of rock by a compression test of an irregular test piece. Int J Rock Mech Min Sci 1966;3:89–99.
[2] Jaeger JC. Failure of rocks under tensile conditions. Int J Rock Mech Min Sci 1967;4:219–27.
[3] ISRM. Suggested method for determining point load strength. Int J Rock Mech Min Sci 1985;22:51–60.
[4] Fener M, Kahraman S, Bilgil A, Gunaydin O. A comparative evaluation of indirect methods to estimate the compressive strength of rocks. Rock Mech Rock Eng 2005;38:329–43.
[5] Chau KT, Wong RCH. Uniaxial compressive strength and point load strength of rocks. Int J Rock Mech Min Sci 1996;33:183–8.
[6] Wijk G. Some new theoretical aspects of indirect measurements of the tensile strength of rocks. Int J Rock Mech Min Sci 1978;15:149–60.
[7] Costin SL. Damage mechanics in the post-failure regime. Mech Mater 1986;4:149–60.
[8] Goodman RE. Introduction to rock mechanics. 2nd ed. New York: Wiley; 1989.
[9] Chau KT, Wei XX. Spherically isotropic, elastic spheres subject to diametrical point load strength test. Int J Solids Struct 1999;36:4473–96.
[10] Christensen RM. Yield functions, damage states, and intrinsic strength. Math Mech Solids 2000;5:285–300.
[11] Wu SZ, Chau KT. Dynamic response of an elastic sphere under diametral impacts. Mech Mater 2006;39:1039–60.
[12] Seow PEC, Swaddiwudhipong S. Failure surface for concrete under multiaxial load-a unified approach. J Mater Civil Eng 2005;17:219–28.
[13] Muir Wood D. Geotechnical modelling. London: E&FN Spon; 2004.
[14] Bahrami M, Yovanovich MM, Culham JR. A compact model for spherical rough contacts. J Tribol 2005;127:884–9.
[15] Nakata Y, Hyde AFL, Hyodo M, Murata H. A probabilistic approach to sand particle crushing in the triaxial test. Geótechnique 1999;49:567–83.
[16] Grady DE. Shock-wave compression of brittle solids. Mech Mater 1998;29:181–203.
[17] Neville AM, Brooks JJ. Concrete technology. London: Longman; 1987.
[18] Kahraman S. Evaluation of simple methods for assessing the uniaxial compressive strength of rock. Int J Rock Mech Min Sci 2001;38:981–94.